PCCP

RSC Publishing

PAPER

View Article Online
View Journal | View Issue

# Phosphate mediated adsorption and electron transfer of cytochrome *c*. A time-resolved SERR spectroelectrochemical study†

Cite this: *Phys. Chem. Chem. Phys.*, 2013, **15**, 5386

Daiana A. Capdevila,‡ Waldemar A. Marmisollé,‡ Federico J. Williams and Daniel H. Murgida*

Received 18th June 2012,
Accepted 15th August 2012

DOI: 10.1039/c2cp42044a

**www.rsc.org/pccp**

The study of proteins immobilized on biomimetic or biocompatible electrodes represents an active field of research as it pursues both fundamental and technological interests. In this context, adsorption and redox properties of cytochrome *c* (Cyt) on different electrode surfaces have been extensively reported, although in some cases with contradictory results. Here we report a SERR spectroelectrochemical study of the adsorption and electron transfer behaviour of the basic protein Cyt on electrodes coated with amino-terminated monolayers. The obtained results show that inorganic phosphate (Pi) and ATP anions are able to mediate high affinity binding of the protein with preservation of the native structure and rendering an average orientation that guarantees efficient pathways for direct electron transfer. These findings aid the design of Cyt-based bioelectronic devices and understanding the modulation by Pi and ATP of physiological functions of Cyt.



## Introduction

Cytochrome *c* (Cyt) is a soluble monohemic protein that can be regarded as a multi-functional enzyme as it participates in a number of processes of fundamental importance in cellular life and death. Among them, the best documented function is as an electron shuttle between complexes III and IV in the mitochondrial electron transfer chain. Other functions that have been described in more recent years include scavenging of reactive oxygen species (ROS), production of ROS, cardiolipin oxidation during apoptosis and assembly of the apoptosome.[1–5] The different functions appear to be regulated by a variety of mechanisms such as phosphorylation and local electric fields.[1] Moreover, it has been shown that Cyt is able to bind specifically a number of anions, including chloride, phosphate, ATP, ADP, nitrate, sulfate, perchlorate, citrate, and oxalate.[6–26] Ion binding has been reported to affect or modulate properties and processes of Cyt, such as reduction potential,[6,11,13–15] protein folding,[7,9] the so-called alkaline transition,[8] heat stability,[12] electrophoretic and chromatographic behavior,[16,17] binding to Apaf-1,[27,28] and electron transfer kinetics with natural and artificial redox partners.[1,26,29–34] The binding domains for some of these anions have been studied using NMR and computational methods for both the native and chemically modified protein.[17–26]

Cyt has been extensively investigated not only because of the relevance of its multiple biological functions, but also as a model system for establishing the physical basis of protein electron transfer and for the development of technological devices such as sensors. For many of these basic and applied investigations the protein is immobilized on metallic electrodes or nanoparticles coated with biocompatible or biomimetic films, mainly self-assembled monolayers (SAMs) of ω-functionalized alkanethiols on gold and silver. Cyt is a basic protein with net positive charge at neutral pH,[16] mainly determined by a ring of lysine residues surrounding the partially exposed heme edge, which constitutes the site for electrostatic binding to the natural redox partners in the mitochondrial electron transfer chain. Thus, a usual strategy for immobilization consists of its electrostatic adsorption on SAMs of ω-carboxyl-alkanethiols[35–51] and other negatively charged functional groups such as phosphonate and sulfonate.[42,52] Surprisingly, it has been reported that Cyt is also able to bind efficiently the positively charged surfaces of electrodes coated with SAMs of amino- and trimethylammonium-terminated alkanethiols and to exhibit good electrochemical response in the assemblies.[42] In a more recent work it was concluded that adsorption of Cyt

*Departamento de Química Inorgánica, Analítica y Química Física and INQUIMAE, Facultad de Ciencias Exactas y Naturales, Universidad de Buenos Aires and CONICET, Ciudad Universitaria pab. 2, piso 3, C1428EHA-Buenos Aires, Argentina. E-mail: dhmurgida@qi.fcen.uba.ar; Fax: +54 11 4576-3341*

† Electronic supplementary information (ESI) available: XPS and SERR data. See DOI: 10.1039/c2cp42044a

‡ Both authors contributed equally.

to amino-terminated SAMs occurs through the protein side opposite to the partially exposed heme.[53] This proposal, however, is not compatible with the good electrochemical response reported previously.[42] On the other hand, no protein adsorption was reported on cysteamine SAMs employed for studying nanoparticle enhancement of long-range electron transfer of Cyt.[54] Contradictory results have also been reported regarding the possibility of adsorbing Cyt to other surfaces such as SAMs of mercaptopyridine and OH-terminated alkanethiols.[55–61]

Clarifying the ability of Cyt to bind different types of surfaces and characterizing the redox properties of the protein in these complexes are issues of great interest as this knowledge will contribute to a better understanding of the interactions of Cyt with the different biological partners and with the building blocks employed in biomimetic and technological devices.

In this work we have investigated the interactions of Cyt with amino-terminated SAMs. Using stationary and time-resolved surface-enhanced resonance Raman (SERR) spectroelectrochemistry, as well as cyclic voltammetry (CV) and X-ray Photoelectron Spectroscopy (XPS), we determined that Cyt is unable to bind efficiently to amino-terminated SAMs at neutral pH, but inorganic phosphate and ATP mediate the adsorption with high affinity and specificity. Moreover, the adsorbed protein retains the native structure, is electrochemically active and adopts similar orientations on $NH_2$- and COOH-terminated SAMs, thus leading to comparable electron transfer dynamics.

## Experimental section

### Chemicals

Cysteamine hydrochloride ($NH_2$-C2), 6-mercaptohexanoic acid (COOH-C6), 6-mercapto-1-hexanol (OH-C6), 8-mercapto-1-octanol (OH-C8), 11-mercapto-1-undecanol (OH-C11) and adenosine 5-triphosphate magnesium salt (ATP) purchased from Sigma-Aldrich; 6-amino-1-hexanethiol hydrochloride ($NH_2$-C6), 8-amino-1-octanethiol hydrochloride ($NH_2$-C8), 11-amino-1-undecanethiol hydrochloride ($NH_2$-C11), and 11-amino-1-hexadecanethiol hydrochloride ($NH_2$-C16) purchased from Dojindo; and 16-mercapto-1-hexadecanol (OH-C16) purchased from Frontier Scientific were all used without further purification. Horse heart cytochrome *c* (Cyt) purchased from Sigma-Aldrich was twice filtered (Millipore Amicon 10 kDa) in buffer solution. All chemicals were of the highest available purity. Aqueous solutions were prepared with high purity deionized water (Millipore; 18.2 MΩ).

### Electrochemical experiments

Cyclic voltammetry was performed using a Gamry REF 600 electrochemical workstation. The three-electrode electrochemical cell was equipped with a polycrystalline Au bead (*ca.* 3 $mm^2$) as a working electrode, a Pt wire counter electrode and a Ag/AgCl (3 M KCl) reference electrode to which all potentials cited in this work are referenced.

Unless stated otherwise, the supporting electrolyte was 10 mM phosphate buffer (Pi) solution at pH 7.0. All experiments were carried out at room temperature.

### Surface-Enhanced Resonance Raman (SERR) spectroelectrochemistry

SERR spectra were measured with the 514 nm line of an Ar ion laser (Coherent Innova 70C) using a single stage spectrograph (Jobin Yvon HR800) coupled to a confocal microscope (Olympus BX41) and equipped with a liquid-nitrogen cooled CCD detector. Rayleigh scattering was rejected using a razor edge filter (Semrock). The laser radiation was focused onto the surface of a rotating Ag electrode by means of a long-working-distance objective (20×, numerical aperture 0.35). Typically, experiments were performed with a laser power of 12 mW at the sample. The spectroelectrochemical cell for SERR determinations has been described elsewhere.[62]

For time-resolved experiments (TR-SERR), potential steps of variable height and duration were applied to trigger the redox reaction, which was monitored by SERR spectra recorded at variable delay times after each step. Synchronization of potential steps and measuring-laser pulses was achieved by a BNC565 pulse-delay generator. Measuring pulses were generated by passing the cw laser beam through two consecutive laser intensity modulators (Linos).

Subsequent to polynomial background subtraction, SERR spectra were subjected to band fitting analysis using home-made software.

### X-ray photoelectron spectroscopy

XPS measurements were performed under UHV conditions (base pressure $< 5 \times 10^{-10}$ mbar) using a SPECS UHV spectrophotometer system equipped with a 150 mm mean radius hemispherical electron energy analyser and a nine channeltron detector. Spectra were acquired at a constant pass energy of 20 eV using an un-monochromated MgKα (1253.6 eV) source operated at 12.5 kV and 20 mA and a detection angle of 30° with respect to the sample normal on grounded conducting substrates. Quoted binding energies are referenced to the Au $4f_{7/2}$ emission at 84 eV. Atomic ratios were calculated from the integrated intensities of core levels after instrumental and photoionization cross section correction.

### Electrode modification

Ag ring electrodes employed for SERR measurements were treated by repetitive oxidation/reduction electrochemical cycles in 0.1 M KCl to create a SER-active nanostructured surface.

Au electrodes used for CV were first oxidized in 10% $HClO_4$ applying a potential of 3 V for 2 minutes, then sonicated in 10% HCl for 15 minutes, rinsed with water and subsequently treated with a 3 : 1 v/v $H_2O_2$ : $H_2SO_4$ mixture at 120 °C. Finally, electrodes were subjected to repetitive voltammetric cycles between −0.2 and 1.6 V in 10% $HClO_4$ and thoroughly washed with water and ethanol.

For SAM-coating, Ag and Au electrodes were soaked overnight at 4 °C in 2 mM solutions of single component or mixed alkanethiols in 4 : 1 v/v $C_2H_5OH$ : $HClO_4$ $10^{-4}$ M (pH = 4). Mixed SAMs of $NH_2$- and OH-terminated alkanethiols were prepared by varying the relative concentrations of the two components

in the incubation solution. The relative mol fraction of $NH_2$-terminated thiols in the soaking solutions, $x$, is used throughout this work to denominate the different mixed SAMs as $(NH_2)_x(OH)_{1-x}$-C$n$, where $n$ refers to the number of C atoms. Prior to protein adsorption the modified electrodes were rinsed thoroughly with ethanol and water and activated electrochemically as previously described.[51]

For SERR experiments Cyt was directly added to the spectroelectrochemical cell to achieve a final concentration of about 0.15 μM. Adsorption equilibrium was monitored spectroscopically and was achieved typically after a few minutes. SAM-coated Au bead electrodes employed for CV experiments were incubated overnight at 4 °C in 1 mM Cyt solution prior to electrochemical measurements in protein free buffer solutions.

## Results and discussion

### Phosphate mediated adsorption of Cyt

Adsorption of Cyt on nanostructured Ag electrodes coated with SAMs of amino-terminated alkanethiols at neutral pH was investigated by SERR, which allows for the sensitive and selective detection of Cyt molecules in close contact with the surface. For that purpose, SAM-coated electrodes were incubated at open circuit (OC) in 0.15 μM Cyt solutions in pure water or with the addition of 10 mM concentration of one of the following electrolytes: KCl, $KNO_3$, $K_2SO_4$, TrisCl buffer and HEPES buffer. In all cases SERR experiments performed after 60 minutes incubation show extremely weak or no Cyt signal. These results are not unexpected considering that both Cyt[16] and amino-terminated SAMs[63,64] are positively charged to some extent at pH 7. Interestingly, as shown in Fig. 1A for a $NH_2$-C6 SAM, addition of phosphate buffer (Pi; pH 7.0) to any of the previous solutions to obtain a final concentration of 10 mM results in the appearance of strong Cyt SERR signals, which become constant within a few minutes after Pi injection. Consistently, direct incubation of the electrodes in Cyt solutions containing increasing concentrations of Pi yields increasing amounts of adsorbed protein up to a maximum Pi concentration of *ca.* 7 mM (Fig. 1B). Further increase of Pi concentration in the incubation solutions results in a decrease of Cyt SERR signal, which becomes very weak for ionic strengths above 150 mM (Fig. 1C). On the other hand, addition of increasing amounts of $KNO_3$ to electrodes previously incubated in Cyt solutions containing 10 mM Pi solutions leads to a sharp decrease of the signal (Fig. 1C) that nearly disappears at $KNO_3$ concentrations above 100 mM.

These results constitute a clear indication that Pi-mediated adsorption of Cyt to $NH_2$-terminated SAMs involves electrostatic interactions of specific nature, and are consistent with the existence of high affinity sites for Pi on the surface of Cyt, as shown previously.[11,22,65]

In order to assess the Pi-mediated affinity of Cyt for $NH_2$-terminated SAMs in a quantitative manner, $NH_2$-C6 coated electrodes were incubated in 10 mM Pi solutions of variable Cyt concentration. The bulk concentration of Cyt was determined by UV-vis absorption, while the relative surface concentration

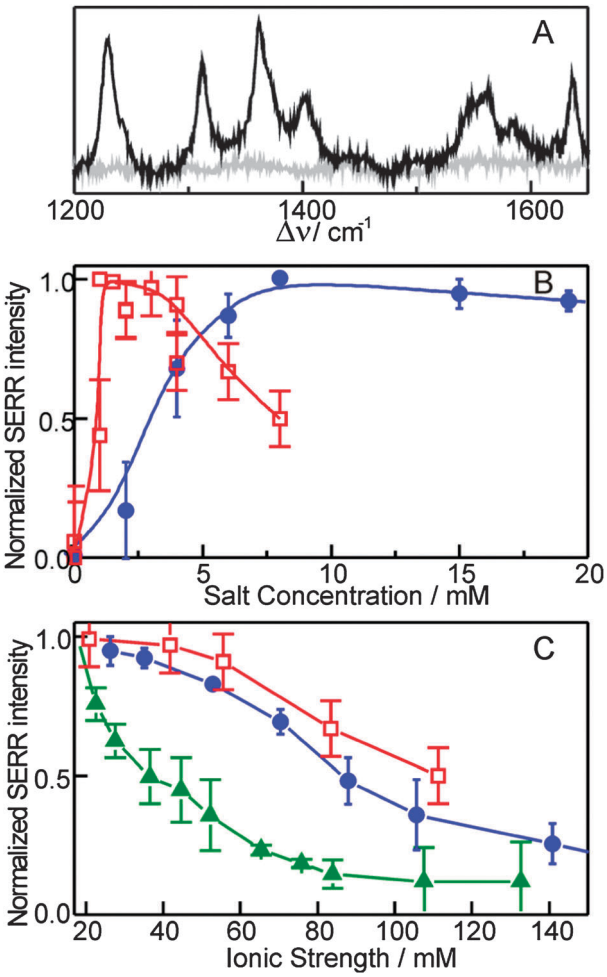


**Fig. 1** Adsorption of Cyt on $NH_2$-C6 SAMs at OC. (A) SERR spectra in the absence (grey) and presence (black) of 10 mM phosphate. (B) Normalized SERR intensity as a function of ATP (squares) and Pi (circles) concentration. (C) Normalized SERR intensity as a function of the ionic strength achieved by adding different salts to a 10 mM Pi solution: ATP (squares), Pi (circles), and $KNO_3$ (triangles).

was monitored by SERR measurements performed as a function of incubation time to ensure equilibrium conditions, which were achieved after approximately 7 minutes. Experiments were performed at two extreme applied electrode potentials, −200 and 150 mV, to ensure full reduction and full oxidation of the adsorbed protein, respectively.

For the sake of comparison, identical experiments were performed to monitor the adsorption of Cyt to COOH-C6 coated electrodes. At neutral pH these SAMs are partially deprotonated and have been extensively reported as suitable platforms for efficient Cyt adsorption.[35–51]

The experimental data were treated in terms of eqn (1), where $I$ is the SERR intensity, $K$ is the affinity constant, $I_{max}$ is the intensity under saturation conditions and [Cyt] is the concentration of the protein in the bulk solution.

$$I = I_{max}\frac{K[\mathrm{Cyt}]^n}{1 + K[\mathrm{Cyt}]^n} \quad (1)$$

 

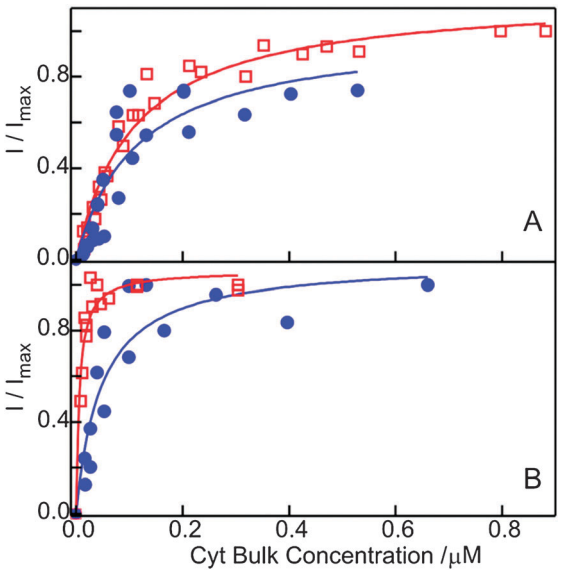


**Fig. 2** SERR normalized intensity of Cyt bands on $NH_2$-C6 (squares) and COOH-C6 (circles) as a function of Cyt bulk concentration in 10 mM Pi buffer pH 7. (A) $E = -200$ mV, (B) $E = 150$ mV.

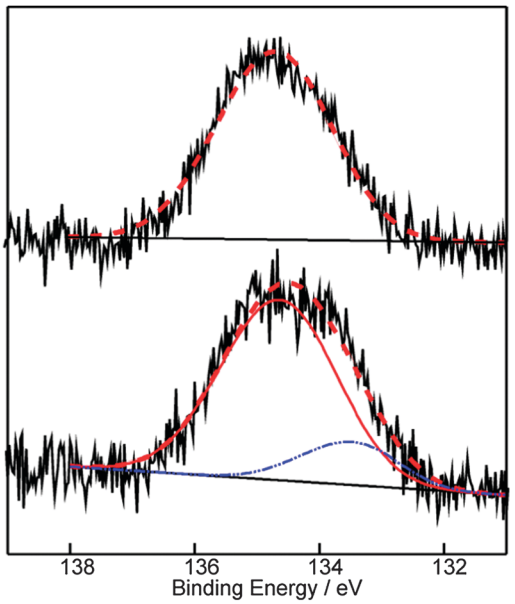


**Fig. 3** P 2p XPS spectra of $(NH_2)_{0.5}(OH)_{0.5}$-C6 SAM modified gold electrode incubated overnight in 0.5 M ATP (top) and 1 mM Cyt in 0.5 M ATP solution (bottom).

As shown in Fig. 2 and Table 1, the data could be adjusted reasonably well with eqn (1) for both types of SAMs and redox states of the protein, yielding *n* values close to 1 within error, as expected for a simple Langmuir adsorption model.

Notably, the affinity of ferrous Cyt ($Cyt^{2+}$) for $NH_2$-terminated SAMs in the Pi-mediated adsorption process is similar to that obtained for direct electrostatic adsorption to COOH-terminated SAMs and to the values previously reported for adsorption on silica.[66] In contrast, for the ferric form ($Cyt^{3+}$) the affinity is one order of magnitude higher in the Pi-mediated process (Table 1). These results are consistent with the higher affinity of $Cyt^{3+}$ for Pi compared with $Cyt^{2+}$, as determined in previous studies in solution.[11]

Adsorption of Cyt to $NH_2$-terminated SAMs can also be mediated by ATP even more efficiently than by Pi. As shown in Fig. 1B, maximum Cyt surface concentration is obtained at ATP concentrations close to 1 mM, *i.e.* one order of magnitude less than for Pi-mediated adsorption. Further addition of ATP produces Cyt desorption, although the effect is slightly less pronounced than for Pi (Fig. 1C).

Fig. 3 shows XPS P 2p signals obtained for electrodes incubated overnight in aqueous solution of ATP and ATP plus Cyt, respectively. In both cases P 2p signals are clearly observed with a main peak at 284.8 eV, indicating that ATP adsorbs on the coated electrodes. Note that the peak is asymmetric only for the electrodes incubated with Cyt, suggesting that the protein interacts with ATP affecting the binding energy of the P 2p electrons giving rise to a new component at 133.2 eV ($P^{Cyt}$). The surface concentration of Cyt can be estimated from the C 1s signal at 288.3 eV (Fig. S1, ESI†) that corresponds to C atoms from acid derivatives ($C^{COX}$). The relative intensities of the $C^{COX}$ (288.3 eV) and $P^{Cyt}$ (133.2 eV) signals indicate the presence of 1.3 ATP molecules per Cyt on the electrode surface. On the other hand, the normalised intensity ratios of the $C^{COX}$ and N 1s signals are 126 and 166, respectively (Fig. S2, ESI†), *i.e.* very close to the stoichiometry expected for the protein ($C^{COX}_{126}:N_{148}$), thus indicating that the contribution of the N1s signal from the alkanethiols is small. Therefore, XPS results suggest the existence of approximately 1 : 1 ATP–Cyt complexes adsorbed on the SAM-coated electrodes.

**Table 1** Adsorption parameters of Cyt on $NH_2$ and COOH-SAMs in phosphate buffer 10 mM pH 7

| | $NH_2$-C6 | | COOH-C6 | |
|---|---|---|---|---|
| *E*/mV | $K/\mu M^{-1}$ | *n* | $K/\mu M^{-1}$ | *n* |
| −200 | 9 ± 2 | 1.4 ± 0.1 | 9 ± 3 | 1.5 ± 0.3 |
| 150 | 160 ± 50 | 1.2 ± 0.2 | 20 ± 5 | 1.2 ± 0.2 |

## Structure, orientation and redox equilibrium of adsorbed Cyt

Resonance Raman (RR) and SERR spectra of heme proteins are very sensitive probes of the structural integrity of the heme redox active site. Specifically, the marker bands region (*ca.* 1300–1700 $cm^{-1}$) is particularly indicative of changes in the redox state, spin and coordination pattern of the heme iron.[48,49,62] As shown in Fig. 4, SERR spectra of Cyt adsorbed to an electrode coated with $NH_2$-C6 sensitively respond to the applied potential, indicating that the immobilized protein is electrochemically active. Furthermore, SERR recorded at sufficiently negative or positive potentials are identical to the RR spectra recorded in solution for native $Cyt^{2+}$ and $Cyt^{3+}$, respectively, in terms of peak positions and bandwidths. The differences in relative intensities of RR and SERR spectra are due to the isotropic character of the solution that contrasts with the anisotropy of the adsorbed protein, and the different spectroscopic

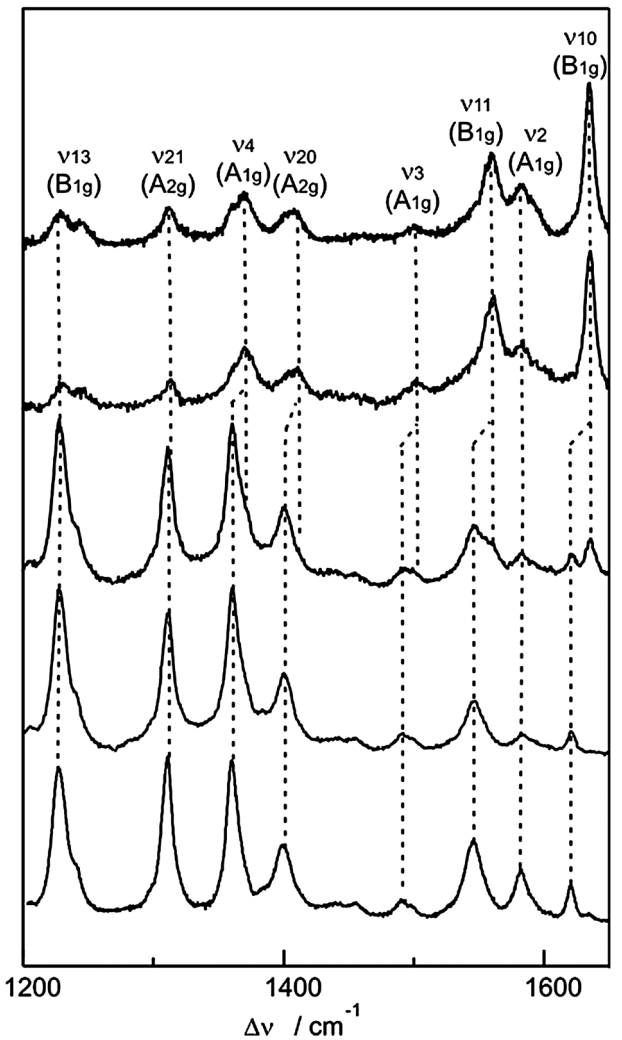


**Fig. 4** RR and SERR spectra of Cyt obtained with 514 nm excitation. From top to bottom: RR of $Cyt^{3+}$, SERR of Cyt adsorbed on $NH_2$-C6 in 10 mM Pi buffer at 200 mV, 70 mV and −200 mV; RR of $Cyt^{2+}$. Band assignment adopted from ref. 67.

selection rules that apply in the two types of experiments. Thus, the comparison of RR and SERR spectra indicates that the protein adsorbs in some preferential orientation and that the structure of the redox active site is well preserved upon immobilization. One should note, however, that small amounts of non-native Cyt species that are not easily detected under Q-band excitation cannot be completely ruled out.

Similar results were obtained for single component ($NH_2$-C*n*) and mixed SAMs (($NH_2$)$_x$ (OH)$_{1-x}$-C*n*) of various chain lengths (*n* = 2, 6, 8, 11 and 16). Moreover, for all SAM compositions and electrode potentials explored, SERR spectra could be quantitatively simulated using the RR spectra of $Cyt^{2+}$ and $Cyt^{3+}$ as spectral components and the intensities as the only adjustable parameters (Fig. S3, ESI†). This treatment allows for the determination of surface relative concentration of $Cyt^{2+}$ and $Cyt^{3+}$ as a function of the applied potential and, thereby, for the determination of formal reduction potentials ($E^\circ$) from Nernst plots (Fig. S4, ESI†). $E^\circ$ values were also determined by CV of Cyt adsorbed on Au electrodes coated with identical SAMs, yielding similar results (Table 2).

**Table 2** Formal redox potential of Cyt adsorbed on different amino-terminated SAMs in 10 mM phosphate buffer pH 7. The standard deviation of the values is less than 10 mV in all cases

| | $E^\circ$/mV (*vs.* Ag–AgCl, KCl 3 M) | | | | |
|---|---|---|---|---|---|
| SAM | *n* = 2 | *n* = 6 | *n* = 8 | *n* = 11 | *n* = 16 |
| $NH_2$-C*n*[a] | 80 | 70 | 60 | 70 | −10 |
| ($NH_2$)$_{0.75}$(OH)$_{0.25}$-C*n*[b] | N.D. | 51 | 30 | 0 | −10 |
| ($NH_2$)$_{0.5}$(OH)$_{0.5}$-C*n*[b] | N.D. | 43 | 30 | 20 | −10 |
| ($NH_2$)$_{0.25}$(OH)$_{0.75}$-C*n*[b] | N.D. | 50 | 50 | 70 | −20 |

[a] Determined by SERR. [b] Determined by CV.

For all SAM compositions the measured $E^\circ$ values vary linearly with the number of methylene groups (Table 2 and Fig. 5), and the values recorded at the thinner SAMs are very close to those reported for Cyt in solutions under otherwise comparable conditions. A very similar behavior has been reported previously for Cyt electrostatically adsorbed on Ag electrodes coated with ω-carboxyl alkanethiols of variable length, and was ascribed to the potential drop across the SAM.[48,49,62] The similarities between COOH- and $NH_2$-terminated SAMs indicate that the two types of systems present comparable interfacial potential distributions, thereby reinforcing the idea that Pi binds to Cyt and to the $NH_2$-terminated SAMs overcompensating the partial positive charges of the electrode coating.

As recently demonstrated, the average orientation of the heme group of adsorbed Cyt with respect to the electrode surface can be inferred from the relative intensities of SERR bands of different symmetry recorded under Q-band excitation.[47] Specifically, $A_{1g}$ totally symmetric modes are preferentially enhanced when the heme plane is parallel to the surface; while for a perpendicular orientation, also the non-totally symmetric modes $A_{2g}$, $B_{1g}$ and $B_{2g}$ are enhanced to a similar extent. Therefore, changes in the average orientation of Cyt on the surface can be monitored through the intensity ratio of SERR bands that correspond to modes of different symmetry.

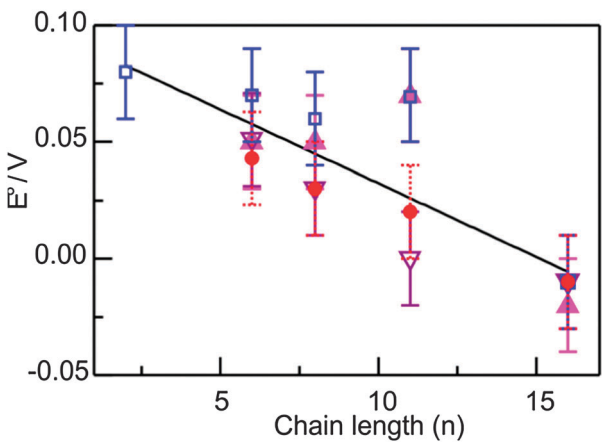


**Fig. 5** Formal redox potential of Cyt adsorbed on different SAMs. Squares: $NH_2$-SAM; circles: ($NH_2$)$_{0.5}$(OH)$_{0.5}$-SAM; up-triangles: ($NH_2$)$_{0.25}$(OH)$_{0.75}$-SAM; down-triangles: ($NH_2$)$_{0.75}$(OH)$_{0.25}$-SAM.

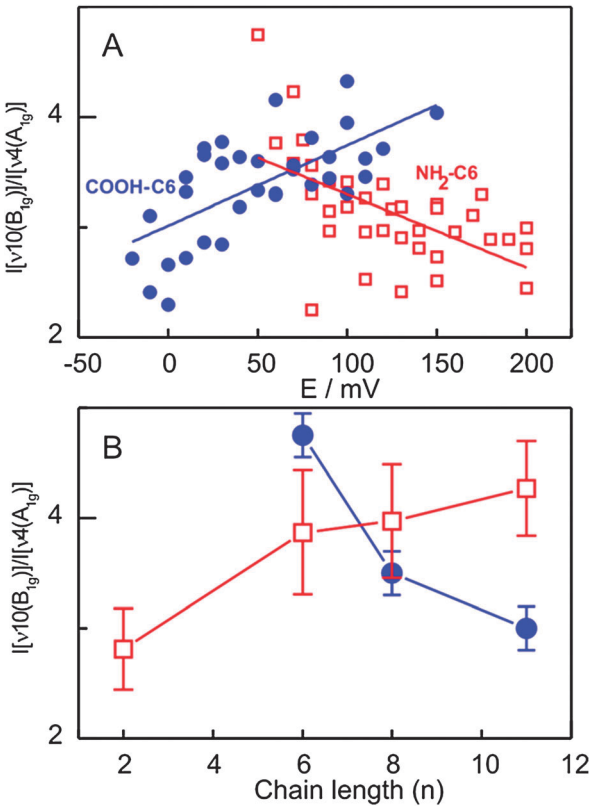


**Fig. 6** Intensity ratio of the $\nu_{10}$ and $\nu_4$ SERR bands for Cyt on $NH_2$-SAMs (squares) and COOH-SAMs (full circles, data taken from ref. 47). (A) Dependence on the applied potential for $n = 6$, (B) values extrapolated to 0 V *vs.* chain length (number of C atoms).

Fig. 6A compares the intensity ratio $I[\nu_{10}(B_{1g})]/I[\nu_4(A_{1g})]$ for $Cyt^{3+}$ adsorbed on $C_6$-COOH and $C_6$-$NH_2$ SAM as a function of the applied electrode potential. The values obtained for both monolayers are within the same range, indicating that direct adsorption of Cyt to negatively charged SAMs and Pi-mediated adsorption to positively charged SAMs involves the same region of the protein surface. The potential dependences of the average orientations, however, follow opposite tendencies: upon increasing the electrode potential, the heme group becomes more perpendicular to the surface on $NH_2$-C6 and more parallel on COOH-C6 SAMs.

The orientation of adsorbed Cyt as a function of the coating thickness also exhibits opposite tendencies for $NH_2$- and COOH-terminated SAMs, with the heme group orienting more perpendicular at thinner $NH_2$-terminated SAMs, and *vice versa* (Fig. 6B).

The orientation of Cyt on the SAM-coated electrodes is determined by the interplay of specific interactions and the alignment of the protein dipole moment with the local electric field. For SAMs with negatively charged ω-functional groups shorter chain lengths or more positive potentials correspond to higher interfacial electrical field.[48,49,62] The opposite tendencies found for Pi-mediated adsorption with respect to direct adsorption to COOH-terminated SAMs may indicate that the binding of Pi produces a displacement of the dipole moment vector of Cyt.

### Kinetics of Pi-mediated electron transfer

Electron transfer dynamics of Cyt adsorbed to the different $NH_2$-terminated SAMs in the presence of 10 mM Pi was investigated by time-resolved SERR spectroelectrochemistry. Experiments were performed by applying potential steps from an initial equilibrium value of *ca.* −100 mV to the formal redox potential of the immobilized protein. SERR spectra were recorded at various delay times after the perturbation and analyzed as described in the previous sections. Fig. 7 shows the time evolution of SERR spectra after a potential step. The spectra can be quantitatively simulated by using only the RR spectra of $Cyt^{2+}$ and $Cyt^{3+}$ as spectral components and adjusting the intensities.

Time-dependent concentration profiles obtained from this analysis exhibit a monoexponential behavior (Fig. S5, ESI†) from where apparent electron transfer rate constants at zero driving force ($k_{app}^0$) were obtained. The electron transfer kinetics of adsorbed Cyt was also investigated by CV. Fig. 8 shows typical voltammograms which exhibit the characteristic linear dependence of the peak intensities with the scan rate, and increasing peak separations that allow the determination of $k_{app}^0$ using Laviron's formalism.[68]

The two techniques yield consistent results for Cyt adsorbed to both single component ($NH_2$-C*n*) and mixed SAMs ($NH_2$-C*n*/OH-C*n*) of variable chain length. The electron transfer

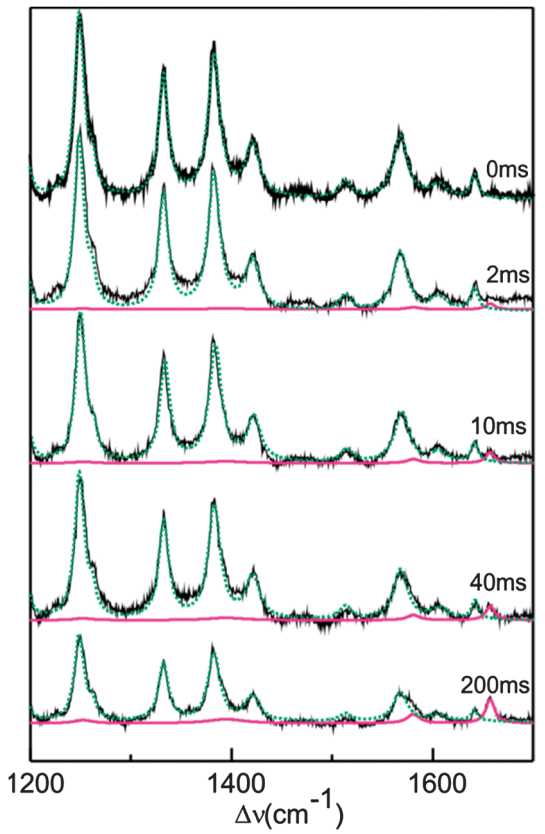


**Fig. 7** Baseline corrected TR-SERR spectra at different delay times for a $NH_2$-C6 coated Ag electrode. The components were obtained from RR spectra of $Cyt^{2+}$ (dashed line) and $Cyt^{3+}$ (full line). Overpotential: −0.1 V.

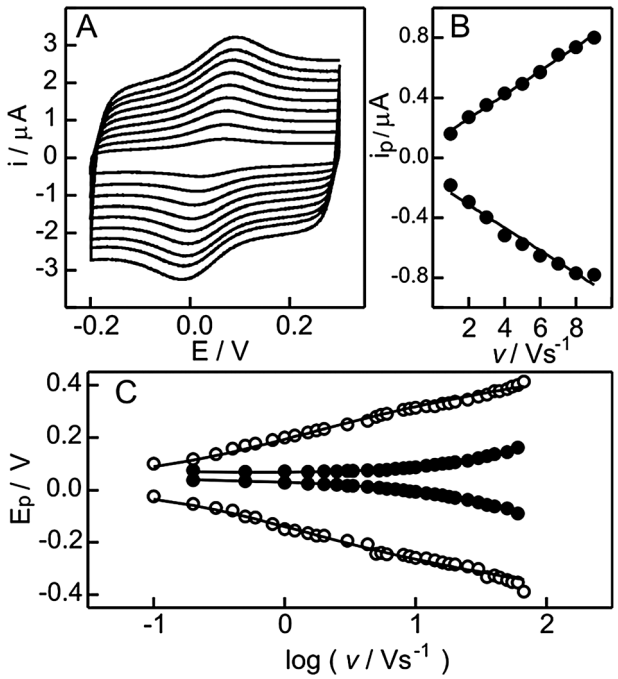


**Fig. 8** (A) Voltammograms of Cyt adsorbed on $(NH_2)_{0.5}(OH)_{0.5}$-C6 in Pi buffer at different scan rates between 1 and 9 V $s^{-1}$. (B) Background corrected peak currents as a function of the scan rate. (C) Voltammetric peak potential of Cyt adsorbed on $(NH_2)_{0.5}(OH)_{0.5}$-SAMs of different chain length as a function of the scan rate: C6 (full circles) and C11 (empty circles).

rate of Cyt increases exponentially upon shortening the length of the spacer, as expected for a single step non-adiabatic reaction, but it becomes distance-independent for the thinner SAMs (Fig. 9).

A similar behavior has been observed for a variety of proteins on different types of SAMs and, particularly, for Cyt on COOH-terminated SAMs.[38,39,43,48,49,69] In this last case the origin of the plateau has been addressed by a combination of experimental and computational techniques, which demonstrated that the rate limiting step in the plateau region is not electron transfer but protein reorientation and thermal fluctuations of the protein and interfacial water molecules that are indispensable for establishing efficient electron pathways. Moreover, it has been shown that both types of motion are strongly influenced by the interfacial electric field.[46,47]

A similar mechanism may hold for Pi-mediated adsorption of Cyt to $NH_2$-terminated SAMs. As shown in Fig. 10A, the apparent electron transfer rates of Cyt are insensitive to the mole fraction of the $NH_2$-component in mixed SAMs of longer alkanethiols. For thinner films, however, $k_{app}{}^0$ decays upon increasing the content of the $NH_2$-component. These results suggest that the partially protonated $NH_2$-groups provide the binding sites for Pi adsorption, which in turn serve as binding sites for Cyt. As a result of Pi adsorption the positive charges of the SAM are overcompensated, yielding a negatively charged surface that presents an interfacial potential distribution qualitatively similar to COOH-terminated SAMs. Therefore, higher contents of $NH_2$-components in the mixed SAMs correspond to higher electric fields that hinder high and low amplitude motion of the adsorbed protein, thereby limiting the rate of heterogeneous electron transfer. In good agreement with this interpretation, measured rates in the plateau region are sensitive to the solution viscosity, which was varied by

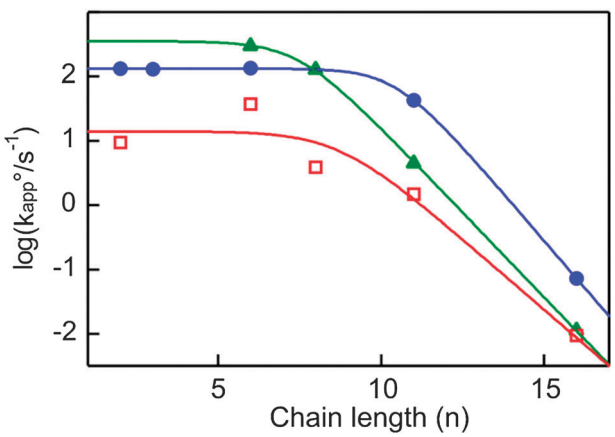


**Fig. 9** Dependence of the apparent electron transfer rate constant on the chain length of the SAM: $NH_2$-C*n* (squares), $(NH_2)_{0.175}(OH)_{0.825}$-C*n* (up triangles), and COOH-C*n* (circles, data taken from ref. 69).

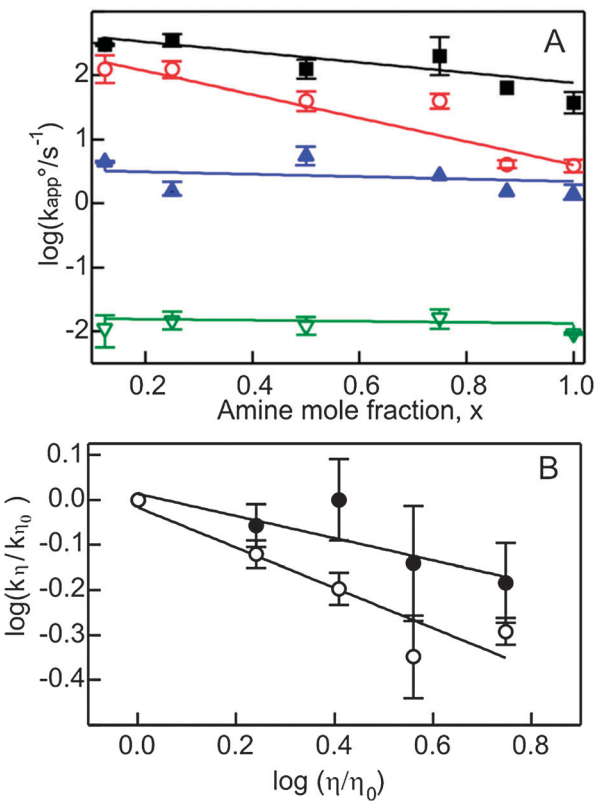


**Fig. 10** (A) Apparent electron transfer rate constant of Cyt as a function of the amine molar fraction, *x*, of the SAM for different chain length: C6 (squares), C8 (empty circles), C11 (up triangles), and C16 (down triangles). Data obtained from CV experiments, except for $x = 1$, that were measured by TR-SERRs. (B) Effect of viscosity on the rate constant of Cyt on $NH_2$/OH-C6 of different composition: $x = 0.125$ (black circles), $x = 0.875$ (empty circles). The subscript ''0'' refers to solution without sucrose.

 

addition of sucrose (Fig. 10B). The effect is more severe for SAMs with higher contents of $NH_2$-groups. In contrast, no viscosity effects were observed for the longer SAMs, independently of the content of $NH_2$-terminated alkanethiols.

Note that the rates of heterogeneous electron transfer of Cyt on COOH- and $NH_2$-terminated SAMs are relatively similar (Fig. 9). The larger differences are observed for single component $NH_2$-terminated SAMs that present reaction rates *ca.* one order of magnitude lower than for COOH-terminated SAMs, which corresponds to electronic couplings that differ only by a factor of three. As previously shown, small rotations of the protein by less than 5° may result in variations of the electronic coupling of more than one order of magnitude. Therefore, one can safely conclude that adsorption of Cyt to the two types of surfaces involves essentially the same protein region.

## Conclusion

In this work we show that phosphate anions and phosphate containing species such as ATP are able to mediate high affinity binding of both $Cyt^{2+}$ and $Cyt^{3+}$ to surfaces containing $NH_2$-groups where adsorption of this basic protein is not expected at physiological pH. SERR experiments show that the orientation of the adsorbed protein is comparable to that observed for adsorption on COOH-terminated SAMs. These results are consistent with the fact that interactions of Cyt with phosphate derivatives in solution have been reported to involve lysine residues 86, 87 and 88, Thr89 and Arg91,[11,19,22,26] while adsorption to COOH-terminated SAMs involves lysines 8, 13, 72, 73, 86 and 87.[46] As shown in Fig. 11, these binding domains are partially superimposed and, therefore, the electronic coupling in both cases is expected to be comparable, as verified by the present time-resolved SERR and CV determinations.

This information is expected to be valuable for the design of molecular bioelectronic devices that include Cyt as a redox active building block. Moreover, it may help to understand the modulation by Pi and ATP of physiological functions of Cyt, such as the assembly of the apoptosome whose structure has not been yet determined at high resolution.[70]

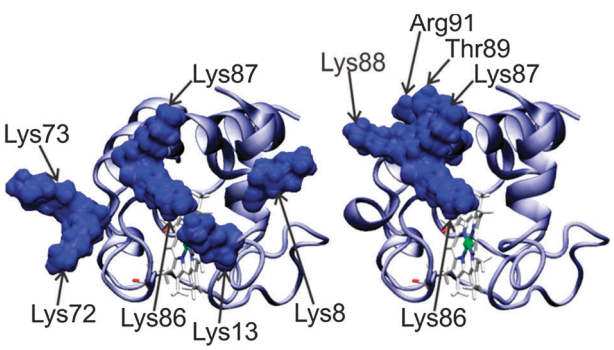


**Fig. 11** Schematic representation of the three-dimensional structures of ferric Cyt (PDB code: 2FRC). The highlighted residues are those involved in the binding to COOH-SAMs (left) and/or phosphate (right). The orientation is the same in both representations.

## Acknowledgements

Financial support from ANPCyT (PICT 2010-070 and PICT 2011-1249) and UBA (UBACYT 20020090100094) is gratefully acknowledged. FJW and DHM are members of CONICET. DAC and WAM thank a fellowship of CONICET.

## Notes and references

1 M. Huttemann, P. Pecina, M. Rainbolt, T. H. Sanderson, V. E. Kagan, L. Samavati, J. W. Doan and I. Lee, *Mitochondrion*, 2011, **11**, 369–381.
2 C. Adrain and S. J. Martin, *Trends Biochem. Sci.*, 2001, **26**, 390–397.
3 X. C. Yu, D. Acehan, J. F. Menetret, C. R. Booth, S. J. Ludtke, S. J. Riedl, Y. G. Shi, X. D. Wang and C. W. Akey, *Structure*, 2005, **13**, 1725–1735.
4 J. M. Stevens, *Metallomics*, 2011, **3**, 319–322.
5 I. Bertini, G. Cavallaro and A. Rosato, *Chem. Rev.*, 2006, **106**, 90–115.
6 G. Battistuzzi, M. Borsari, D. Dallari, I. Lancellotti and M. Sola, *Eur. J. Biochem.*, 1996, **241**, 208–214.
7 S. Zhong, D. L. Rousseau and S. R. Yeh, *J. Am. Chem. Soc.*, 2004, **126**, 13934–13935.
8 G. Battistuzzi, M. Borsari, A. Ranieri and M. Sola, *Arch. Biochem. Biophys.*, 2001, **386**, 117–122.
9 U. Ahluwalia, C. Prakash, R. Agrawal and S. Deep, *Int. J. Biol. Macromol.*, 2011, **49**, 752–760.
10 U. Ahluwalia, S. M. Nayeem and S. Deep, *Eur. Biophys. J.*, 2011, **40**, 259–271.
11 D. Gopal, G. S. Wilson, R. A. Earl and M. A. Cusanovich, *J. Biol. Chem.*, 1988, **263**, 11652–11656.
12 D. U. Ahn and A. J. Maurer, *Poult. Sci.*, 1989, **68**, 1218–1225.
13 R. Margalit and A. Schejter, *Eur. J. Biochem.*, 1974, **46**, 387–391.
14 R. Margalit and A. Schejter, *Eur. J. Biochem.*, 1973, **32**, 492–499.
15 R. Margalit and A. Schejter, *Eur. J. Biochem.*, 1973, **32**, 500–505.
16 G. H. Barlow and E. Margolia, *J. Biol. Chem.*, 1966, **241**, 1473–1477.
17 D. L. Brautigan, S. Fergusonmiller and E. Margoliash, *J. Biol. Chem.*, 1978, **253**, 130–139.
18 D. L. Brautigan, S. Fergusonmiller, G. E. Tarr and E. Margoliash, *J. Biol. Chem.*, 1978, **253**, 140–148.
19 Y. Q. Feng and S. W. Englander, *Biochemistry*, 1990, **29**, 3505–3509.
20 G. Taler, G. Navon and O. M. Becker, *Biophys. J.*, 1998, **75**, 2461–2468.
21 A. D. Karshikov and B. P. Atanasov, *Stud. Biophys.*, 1985, **105**, 23–28.
22 N. Osheroff, D. L. Brautigan and E. Margoliash, *Proc. Natl. Acad. Sci. U. S. A.*, 1980, **77**, 4439–4443.
23 T. Andersson, E. Thulin and S. Forsen, *Biochemistry*, 1979, **18**, 2487–2493.
24 R. A. Morton and K. Breskvar, *Can. J. Biochem.*, 1977, **55**, 146–151.

25 E. Stellwag and R. G. Shulman, *J. Mol. Biol.*, 1973, **75**, 683–695.
26 G. Taborsky and K. Mccollum, *J. Biol. Chem.*, 1979, **254**, 7069–7075.
27 T. N. Yu, X. D. Wang, C. Purring-Koch, Y. Wei and G. L. McLendon, *J. Biol. Chem.*, 2001, **276**, 13034–13038.
28 C. Purring-Koch and G. McLendon, *Proc. Natl. Acad. Sci. U. S. A.*, 2000, **97**, 11928–11931.
29 S. Fergusonmiller, D. L. Brautigan and E. Margoliash, *J. Biol. Chem.*, 1976, **251**, 1104–1115.
30 A. M. English and E. Cheung, *Inorg. Chim. Acta*, 1992, **201**, 243–246.
31 Y. J. Zhen, C. W. Hoganson, G. T. Babcock and S. Ferguson-Miller, *J. Biol. Chem.*, 1999, **274**, 38032–38041.
32 K. F. Wang, Y. J. Zhen, R. Sadoski, S. Grinnell, L. Geren, S. Ferguson-Miller, B. Durham and F. Millett, *J. Biol. Chem.*, 1999, **274**, 38042–38050.
33 M. Huttemann, S. Helling, T. H. Sanderson, C. Sinkler, L. Samavati, G. Mahapatra, A. Varughese, G. R. Lu, J. Liu, R. Ramzan, S. Vogt, L. I. Grossman, J. W. Doan, K. Marcus and I. Lee, *Biochim. Biophys. Acta, Bioenerg.*, 2012, **1817**, 598–609.
34 A. N. Volkov, P. Nicholls and J. A. R. Worrall, *Biochim. Biophys. Acta, Bioenerg.*, 2011, **1807**, 1482–1503.
35 J. S. Xu and E. F. Bowden, *J. Am. Chem. Soc.*, 2006, **128**, 6813–6822.
36 J. Petrovic, R. A. Clark, H. J. Yue, D. H. Waldeck and E. F. Bowden, *Langmuir*, 2005, **21**, 6308–6316.
37 M. J. Tarlov and E. F. Bowden, *J. Am. Chem. Soc.*, 1991, **113**, 1847–1849.
38 A. Avila, B. W. Gregory, K. Niki and T. M. Cotton, *J. Phys. Chem. B*, 2000, **104**, 2759–2766.
39 J. J. Wei, H. Y. Liu, K. Niki, E. Margoliash and D. H. Waldeck, *J. Phys. Chem. B*, 2004, **108**, 16912–16917.
40 H. J. Yue, D. H. Waldeck, K. Schrock, D. Kirby, K. Knorr, S. Switzer, J. Rosmus and R. A. Clark, *J. Phys. Chem. C*, 2008, **112**, 2514–2521.
41 T. D. Dolidze, S. Rondinini, A. Verto-Va, D. H. Waldeck and D. E. Khoshtariya, *Biopolymers*, 2007, **87**, 68–73.
42 X. X. Chen, R. Ferrigno, J. Yang and G. A. Whitesides, *Langmuir*, 2002, **18**, 7009–7015.
43 M. Fedurco, *Coord. Chem. Rev.*, 2000, **209**, 263–331.
44 S. Monari, G. Battistuzzi, M. Borsari, D. Millo, C. Gooijer, G. Van der Zwan, A. Ranieri and M. Sola, *J. Appl. Electrochem.*, 2008, **38**, 885–891.
45 H. K. Ly, M. Sezer, N. Wisitruangsakul, J. J. Feng, A. Kranich, D. Millo, I. M. Weidinger, I. Zebger, D. H. Murgida and P. Hildebrandt, *FEBS J.*, 2011, **278**, 1382–1390.
46 D. Alvarez-Paggi, D. F. Martin, P. M. DeBiase, P. Hildebrandt, M. A. Marti and D. H. Murgida, *J. Am. Chem. Soc.*, 2010, **132**, 5769–5778.
47 A. Kranich, H. K. Ly, P. Hildebrandt and D. H. Murgida, *J. Am. Chem. Soc.*, 2008, **130**, 9844–9848.
48 D. H. Murgida and P. Hildebrandt, *Chem. Soc. Rev.*, 2008, **37**, 937–945.
49 D. H. Murgida and P. Hildebrandt, *Acc. Chem. Res.*, 2004, **37**, 854–861.
50 X. U. Jiang, K. Ataka and J. Heberle, *J. Phys. Chem. C*, 2008, **112**, 813–819.
51 R. Tanimura, M. G. Hill, E. Margoliash, K. Niki, H. Ohno and H. B. Gray, *Electrochem. Solid-State Lett.*, 2002, **5**, E67–E70.
52 Y. Chen, X. J. Yang, L. R. Guo, B. Jin, X. H. Xia and L. M. Zheng, *Talanta*, 2009, **78**, 248–252.
53 Q. M. Yu and G. Golden, *Langmuir*, 2007, **23**, 8659–8662.
54 P. S. Jensen, Q. Chi, F. B. Grumsen, J. M. Abad, A. Horsewell, D. J. Schiffrin and J. Ulstrup, *J. Phys. Chem. C*, 2007, **111**, 6124–6132.
55 M. J. Eddowes and H. A. O. Hill, *J. Chem. Soc., Chem. Commun.*, 1977, **21**, 771–772.
56 K. Ataka and J. Heberle, *J. Am. Chem. Soc.*, 2004, **126**, 9445–9457.
57 H. Yamamoto, H. Y. Liu and D. H. Waldeck, *Chem. Commun.*, 2001, 1032–1033.
58 S. Terrettaz, J. Cheng and C. J. Miller, *J. Am. Chem. Soc.*, 1996, **118**, 7857–7858.
59 S. Monari, A. Ranieri, C. A. Bortolotti, S. Peressini, C. Tavagnacco and M. Borsari, *Electrochim. Acta*, 2011, **56**, 6925–6931.
60 D. Millo, A. Bonifacio, A. Ranieri, M. Borsari, C. Gooijer and G. Van der Zwan, *Langmuir*, 2007, **23**, 4340–4345.
61 N. J. O'Reilly and E. Magner, *Langmuir*, 2005, **21**, 1009–1014.
62 D. H. Murgida and P. Hildebrandt, *J. Phys. Chem. B*, 2001, **105**, 1578–1586.
63 K. P. Fears, S. E. Creager and R. A. Latour, *Langmuir*, 2008, **24**, 837–843.
64 H. Munakata, D. Oyamatsu and S. Kuwabata, *Langmuir*, 2004, **20**, 10123–10128.
65 G. Battistuzzi, M. Borsari and M. Sola, *Arch. Biochem. Biophys.*, 1997, **339**, 283–290.
66 C. M. Kraning, T. L. Benz, K. S. Bloome, G. C. Campanello, V. S. Fahrenbach, S. A. Mistry, C. A. Hedge, K. D. Clevenger, K. M. Gligorich, T. A. Hopkins, G. C. Hoops, S. B. Mendes, H. C. Chang and M. C. Su, *J. Phys. Chem. C*, 2007, **111**, 13062–13067.
67 S. Z. Hu, I. K. Morris, J. P. Singh, K. M. Smith and T. G. Spiro, *J. Am. Chem. Soc.*, 1993, **115**, 12446–12458.
68 E. Laviron, *J. Electroanal. Chem.*, 1979, **101**, 19–28.
69 D. H. Murgida and P. Hildebrandt, *J. Am. Chem. Soc.*, 2001, **123**, 4062–4068.
70 R. Huber, D. Pietsch, T. Panterodt and K. Brand, *Cell. Signalling*, 2012, **24**, 1287–1296.

 

Electronic Supplementary Material (ESI) for Physical Chemistry Chemical Physics


# Phosphate Mediated Adsorption and Electron Transfer of Cytochrome *c*. A Time-Resolved SERR Spectroelectrochemical Study

Daiana Capdevila, Waldemar Marmisollé, Federico J. Williams and Daniel H. Murgida*

## Supplementary Information

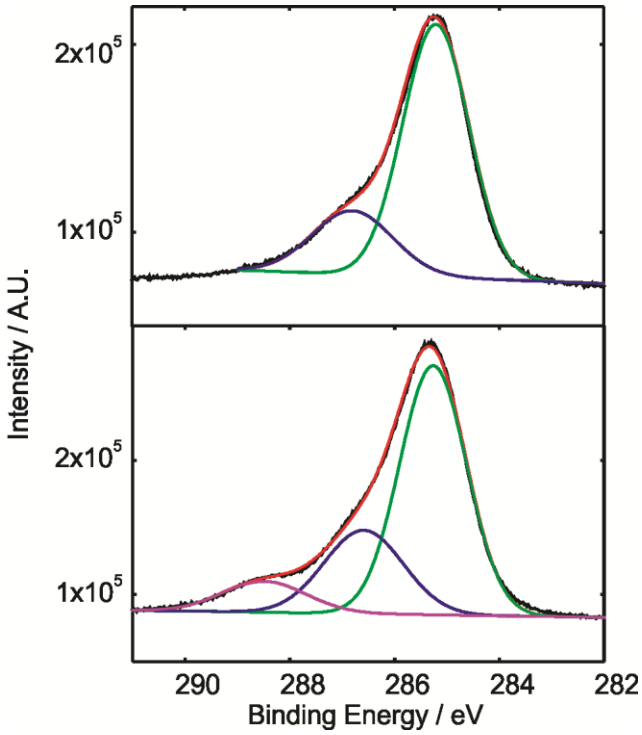


**Figure SI1**. C1s XPS spectra of $(NH_2)_{0.5}$ $(OH)_{0.5}$C6 SAM modified gold electrode incubated overnight in 0.5M ATP (top) and 1mM Cyt in 0.5M ATP solution (bottom).

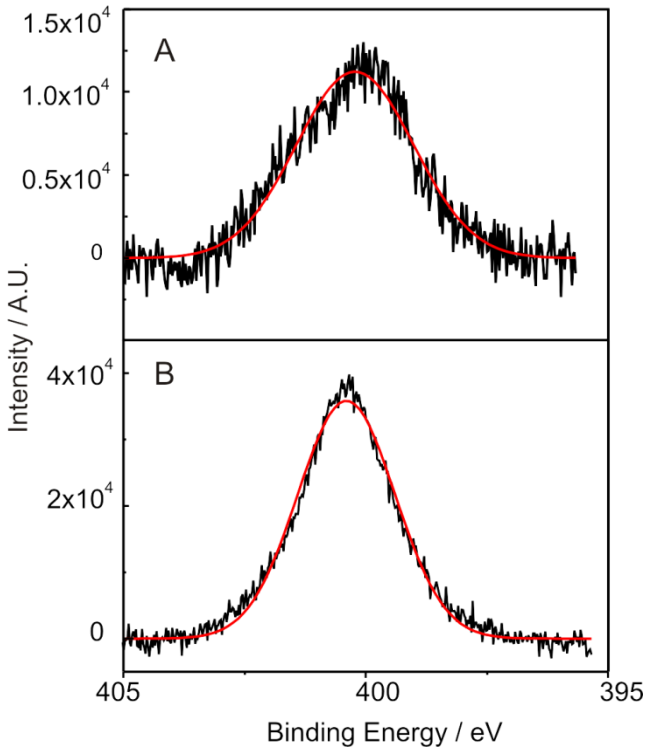


**Figure SI2**. C1s XPS spectra of $(NH_2)_{0.5}$ $(OH)_{0.5}$C6 SAM modified gold electrode incubated overnight in 0.5M ATP (top) and 1mM Cyt in 0.5M ATP solution (bottom).

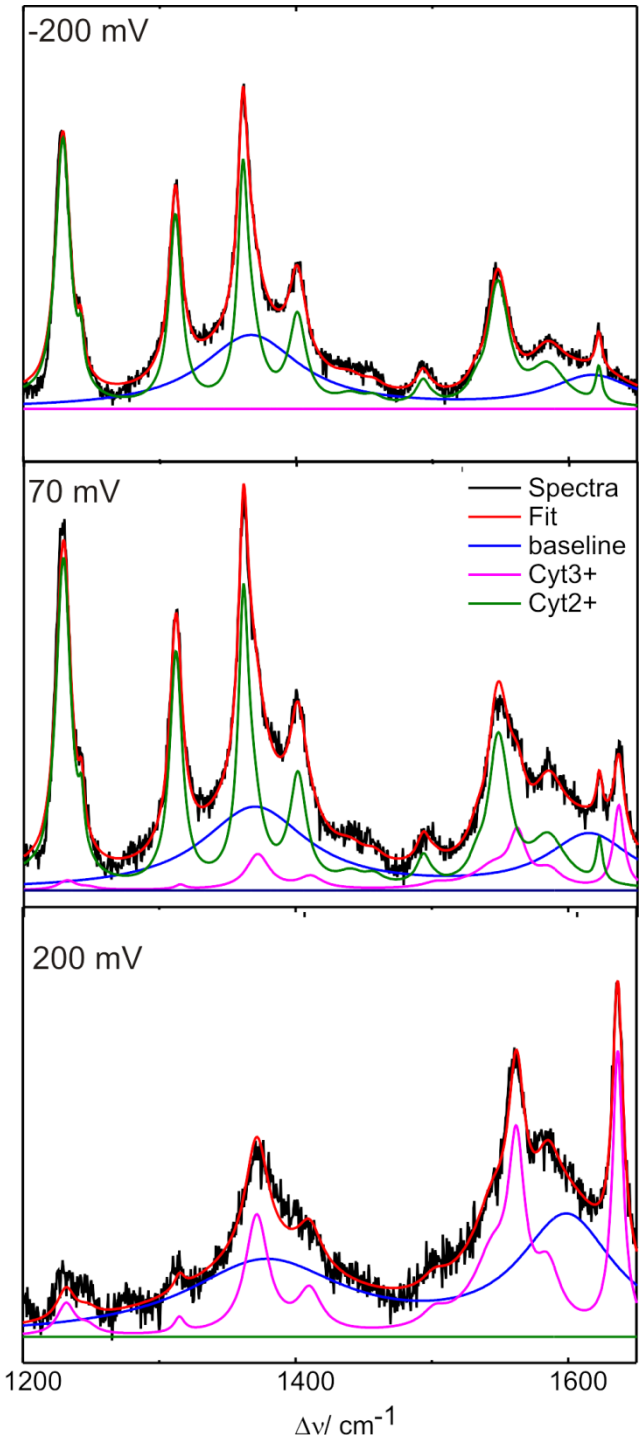


**Figure SI3**. Component analysis of SERR spectra of Cyt on $NH_2$-C6 SAM coated silver electrode at three different applied potentials. The components were obtained from RR spectra of $Cyt^{2+}$ and $Cyt^{3+}$.

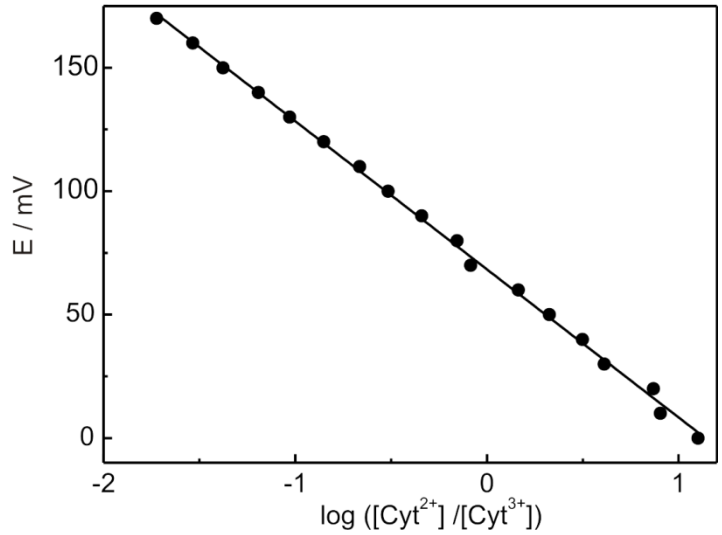


**Figure SI4**. Nernst plot for Cyt on $NH_2$-C6 SAM coated silver electrode. Relative concentrations of reduced and oxidized forms were obtained by component analysis as indicated in Figure SI3.

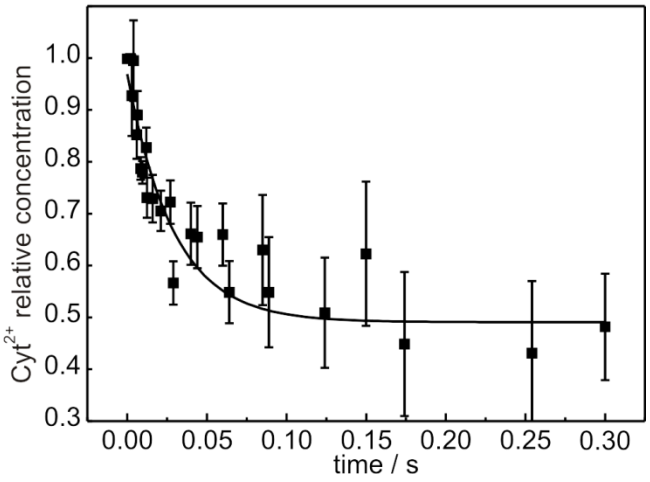


**Figure SI5**. Time dependence of relative concentration of $Cyt^{2+}$ after a potential jump from -100mV to the redox potential for Cyt on $NH_2$-C6 SAM coated silver electrode. Data of two independent experiments are included and fitted to a monoexponential decay function.